Turbulent Mixing Studies In A Secondary Combustor Model

Author(s): J. P. Foote, R. J. Schulzt, T. V. Giel, Jr.

Session Name: Downstream Systems

SEAM: 21 (1983)

SEAM EDX URL: https://edx.netl.doe.gov/dataset/seam-21

EDX Paper ID: 1026

TURBULENT MIXING STUDIES IN A SECONDARY COMBUSTOR MODEL*

J. P. Foote**, R. J. Schulz†, T. V. Giel, Jr.††

Energy Conversion Programs
University of Tennessee Space Institute
Tullahoma, Tennessee 37388

ABSTRACT

A water flow model of the secondary combustor in the Low Mass Flow MHD test train at the U. S. Department of Energy Coal Fired Flow Facility was tested in order to determine the effects of combustor geometry and combustion air injection techniques on the flow and mixing in the secondary combustor. A dual Bragg cell laser velocimeter was used to obtain detailed two-component velocity data for various model configurations, to examine the effects on mixing efficiency of oxidizer injection velocity, oxidizer injection angle and various flow restrictions. The modeling results provide useful insights for the operation of the Coal Fired Flow Facility secondary combustor.

INTRODUCTION

In the open cycle magnetohydrodynamic (MHD) electrical power generation systems tested at The University of Tennessee Space Institute (UTSI), fossil fuels (coal and oil) are burned in a two-stage combustion process to minimize the formation and release of nitrogen oxides (NO_x) to the atmosphere. This two-stage combustion process is employed in the Low Mass Flow (LMF) experimental MHD test train of the U. S. Department of Energy Coal Fired Flow Facility (CFFF) located at UTSI. The LMF primary combustor burns a mixture of pulverized coal and fuel oil, together with K_2CO_3 "seed" to provide an electrically conducting gas for the MHD process. The fuels are burned with stoichiometric ratios ranging from 0.85 to 0.95 at combustion temperatures of about 3000K. Downstream of the MHD channel the gas is cooled slowly in a radiant furnace for thermal NO_x decomposition and exits, at about 1367K, into a secondary combustor where air is added to burn the remaining combustibles, primarily CO and H_2. The gas temperature rises to about 1533K with a stoichiometric ratio of 1.05-1.10 in the secondary combustor allowing the increased thermal energy of the gas to be extracted in a conventional steam generation cycle.

---

*This work was sponsored by the United States Department of Energy under Contract No. DE-AC02-79ET10815

**Research Engineer, Energy Conversion R&D Programs, Member ASME.
†Associate Professor, Member AIAA, ASME.
††Adjunct Professor, Member AIAA, ASME.

The secondary combustor must burn the remaining combustibles efficiently in order to recover as much chemical energy as possible for use in the steam cycle, eliminate the CO species in the gas and minimize NO_x formation. The chemical kinetics of the combustion reactions involving CO and H_2 are much faster than mixing rates of the primary gas and secondary air stream; hence, the mixing effectiveness is the primary factor that determines the combustion efficiency and performance of the secondary combustor.

Because the secondary combustor performance is dominated by fluid mixing phenomena, an experimental program using a 1/6 scale flow model, geometrically similar to the LMF secondary combustor, was undertaken in order to obtain some basic understanding of the mixing and flow in this type of device. By employing a dual Bragg cell laser velocimeter to map the velocity field, detailed velocity and turbulence data were obtained for various combustor geometries and operating conditions. In order to estimate scaling effects for the model, references on the subject of combustion modeling using water as the test fluid were studied. Discussions on water flow modeling were given by Spalding[1] and by Clarke, Gerrard and Holliday[2]. These sources recommend that the bulk velocity ratio and the mass-flow ratio between the two streams entering the model should have the same values as in the real combustor, rather than attempting to match Reynolds numbers or to maintain the areas of the two streams in the same ratio. Data from water flow models scaled in this way have been found to agree well with real combustor performance data, provided that due consideration is given to the effects of spatial density gradients and the temporal density fluctuations produced by chemical reactions or the evolution of heat, which cannot be simulated with cold flow modeling.

The LMF secondary combustor, shown in Figure 1, is a 1.22m square, refractory lined duct. The section where the secondary air is injected has two converging walls which form a 25% (1.22m x 0.91m) restriction in the duct cross section. Passing through each converging wall are two rows of tubes through which air is injected at an angle of 120° relative to the incoming gas flow. Each wall has ten 78.0mm and nine 40.9mm diameter air tubes which can be individually capped to provide many different injector arrangements. The secondary combustor model, shown in Figure 2, was a 203.2mm x 203.2mm square duct constructed from 6.4mm aluminum plate with 3.2mm thick glass windows on one side to allow flow visualization and laser velocimeter measurements. The model was built with separate inlet, mixing and outlet sections so the degree of area restriction in the mixing section could be varied. Three mixing sections were tested, with area reductions of 50%, 25% and 0% (no restriction). Seven holes were located on each converging wall to inject water at either 90° or 120° relative to the bulk flow direction. The hole diameters were adjusted to give the desired velocity ratio between the primary (p) and secondary (s) streams. The five injector/cross section arrangements that were tested are shown in Figure 3.

Based on nominal LMF test conditions, a typical mass-flow-rate ratio ($\dot{m}_s/\dot{m}_p$) for the LMF secondary combustor was found to be fairly constant at about 0.75, so the mass ratio in the model was fixed at a constant value of 0.75 in all tests. Typical bulk velocity ratios (V_s/V_p) for the LMF secondary combustor were found to range from about 10 to 20, so the model tests were conducted with velocity ratios of 10 and 20. In the model study, the primary flow rate was set at 0.0038 m^3/s, resulting in an inlet bulk velocity of 0.092 m/s and an inlet Reynolds number of 1.65×10^4, which is about 30% of the value in the real secondary combustor. The secondary flow injection rate was set at 0.0028 m^3/s. Test conditions for the five cases studied are summarized in Table I.

INSTRUMENTATION

The flow field was measured with a two-component Bragg diffracted laser velocimeter (LV) system, which was designed and constructed at UTSI[3]. The LV measures velocities

TABLE I

SECONDARY COMBUSTOR WATER FLOW MODEL

TEST CONDITIONS[a]

CASE	MASS RATIO ($\dot{m}_{jets}/\dot{m}_{inlet}$)	VELOCITY RATIO (v_{jets}/v_{inlet})	AREA REDUCTION ($\Delta A/A_{inlet}$)	INJECTION ANGLE, β (RELATIVE TO BULK)
1	0.75	20	0.25	120°
2	0.75	10	0.25	120°
3	0.75	20	0.25	90°
4	0.75	20	0.50	120°
5	0.75	20	0.00	120°

[a] Primary flow rate = 0.0038 m^3/s (60gpm). Bulk inlet velocity = 0.092 m/s (0.30 ft/s).
Secondary flow rate = 0.0028 m^3/s (45gpm). Inlet Reynolds number = 1.65 x 10^4

in a flow by detecting the frequency of intensity variations in light scattered by particles as they pass through the interference fringes produced by two intersecting coherent laser beams. The two beams are split from one laser beam using Bragg diffraction, which induces a frequency difference f_b between the intersecting beams. This causes the fringes to move so that a stationary particle in the beam intersection region or "probe volume" scatters light with intensity variations at f_b. The relationship between the measured frequency f and the velocity u is

$$u = \delta(f_b - f) \qquad (1)$$

where δ is the fringe spacing, determined by the geometry of the LV optical train. Thus, the sign as well as the magnitude of the velocity component u is determined. For this study four coherent frequency shifted beams were generated from a single 514.5 nm argon ion laser beam using a two-component, water filled Bragg cell. The four beams formed the corners of a rectangle, with the horizontally separated beams being frequency shifted by 15 MHz and the vertically separated beams shifted by 45 MHz. These four beams were focused at the probe volume, as shown in Figure 4, producing two orthogonal sets of fringes, the horizontal set crossing the center of the probe volume at 15 MHz and the vertical set crossing at 45 MHz. The horizontal fringe spacing, δ_x, was 25.73 μm and the vertical spacing, δ_y, was 8.46 μm. A large off-axis backscatter collector lens focused scattered light from the probe volume onto an aperture in front of a photomultiplier tube. The pulsing light scattered by a particle in the probe volume was converted by the photomultipler tube, into electrical pulses. The electrical pulse frequencies from the horizontal velocities are centered about 15 MHz and from the vertical velocity are centered about 45 MHz. The resulting simultaneous, frequency-separated pulses allow electronic signal separation of the two orthogonal velocity components. The optical system was mounted on a bed that traversed in three orthogonal directions. Each traversing axis was equipped with a digital position indicator with magnetically encoded scales which were used to position the optical train to within $\pm$ 0.05 mm of a desired location.

The LV signal processor was based on a Z80 microprocessor, which allowed on-line data reduction. The raw signal from the photomultiplier tube was divided into equal parts by a signal splitter. Each part was mixed with the output of a local oscillator. One oscillator was operated near 15 MHz and the other was operated near 45 MHz. The output signal from each mixer was low-pass filtered to pass only the difference frequency between the raw signal and the local oscillator. The signals for the horizontal (15 MHz) and vertical (45 MHz) channels were thus separated and the signal

frequencies were significantly lowered, allowing more accurate signal processing. The processors measure the average period of the signals by counting the number of cycles of a 100 MHz clock during some fixed number (usually 8) of signal cycles.

For each measurement location the LV provided 1300 to 1400 simultaneous measurements of instantaneous axial and vertical velocities, u and v. An error analysis determined that the uncertainty in the instantaneous velocities generally ranged from 2% to 4% of the measured values[4]. Statistical methods were used to obtain mean velocities, $\overline{u}$ and $\overline{v}$, turbulence velocities, u' and v', and the cross correlation $\overline{u'v'}$. In general statistical tolerances for the mean and turbulence velocities establish, with 95% probability, that true values are within about 5% of calculated values for each of the ~400 locations per test case. Typical tolerances are presented in Table II.

Table II TYPICAL LASER VELOCIMETER MEASUREMENT CONFIDENCE TOLERANCES

AXIAL				VERTICAL			
$\overline{u}$ (m/s)	$\Delta\overline{u}$(%) tolerance	u' (m/s)	$\Delta u'$(%) tolerance	$\overline{v}$ (m/s)	$\Delta\overline{v}$(%) tolerance	v' (m/s)	$\Delta v'$(%) tolerance
-.741	±4.0	.546	±3.8	-.575	±3.7	.398	±3.8
-.511	2.2	.216	12.5	-.050	38.0	.364	0.3
-.068	25.0	.314	3.2	-.039	43.6	.318	3.1
.070	17.1	.224	4.0	.203	16.7	.618	2.8
.226	7.5	.317	3.8	.305	4.6	.260	5.4
.318	4.7	.281	3.6	.746	3.2	.451	6.2
.492	4.1	.368	2.4	1.367	1.8	.439	4.3
.637	.17	.210	3.8	1.614	1.4	.544	2.6

$f_{bx} = 0.44$ Mhz
$\delta_x = 25.73\ \mu$m
-1.76 m/s $< u <$ 1.53 m/s

$f_{by} = 1.47$ Mhz
$\delta_y = 8.46\ \mu$m
-4.47 m/s $< v <$ 4.47 m/s

RESULTS AND DISCUSSION

Figure 5 shows the mean velocity field in the plane bisecting a jet for one of the model configurations studied. In this case the jet injection angle was 90°, the velocity ratio was 20 and the area reduction in the duct was 25%. The bulk velocities of the incoming primary flow and the secondary (jet) flow were 0.092 m/s and 1.840 m/s respectively.

Examination of Figure 5 shows that the inlet velocity profile was not uniform. This non-uniformity results because the flow entering the combustor turns through a right angled bend. To guarantee a steady inlet velocity profile and allow examination of the injection jet mixing effects separated from the inlet profile effects, an upstream flow-straightener with a coarse mesh was installed. The flow straightener did not eliminate the inlet profiles but produced a similar inlet profile in all cases studied. However, the data analysis indicated that the inlet profile nonuniformity had no significant effects in the combustor mixing regions. Furthermore, in all cases where the velocity ratio was 20, the mass flow in the injection and downstream regions was symmetric about the centerline. In these cases most measurements were made below

the centerline with a few measurements made above the centerline for reference purposes. In the case plotted in Figure 5 recirculation zones were formed both upstream and downstream of the secondary air injection jets.

Figure 6 shows typical flow patterns in different planes around the jets. The figure shows that much of the primary flow was entrained by the jets as it was forced between them. Moreover, the three-dimensional aspects of the flow were confined to the region very near where the jets enter the combustor, such that velocities and turbulence intensities were quite similar across the bulk of the flow. For this reason succeeding plots show data for only the plane bisecting a jet.

The flow was found to have a periodic wake regime in all cases studied. Figure 7 shows a vertical velocity-time history at a point on the centerline of the duct for the case plotted in Figure 5 as well as a frequency spectrum plot which defines the dominant frequency of the flow oscillations. Observation of the flow indicated that the periodic wake regime resulted from the alternate growth and shedding of vortices produced by interaction of the jets and the bulk flow. Primary frequencies ranging from 0.7 to 1.6 Hz were observed and a dependence on the duct area reduction was indicated, but no trend could be established when comparing cases where the area reduction was varied. In the wake regime the time averaged data encompasses this periodic vortex shedding and therefore is not representative of a typical flow pattern. The remainder of the field is a stationary, non-periodic turbulent flow, so there the time averaged data is representative of the typical flow pattern.

Figure 8 shows profiles of mean velocity and turbulence intensity. The bulk velocity of the incoming primary flow (0.092 m/s) was used to normalize the data. The highest turbulence level was found near the jets, and the turbulence intensity profiles became uniform as the flow moved downstream. Mean velocity measurements obtained above the duct centerline are plotted to illustrate the flow symmetry for this case. Figure 9 shows contours of turbulent kinetic energy and Reynolds stress. The highest values of turbulent kinetic energy and Reynolds stress were seen where the jets entered the duct and near the center of the duct where the opposing jets interacted.

Figure 10 shows a comparison of two test cases where the bulk velocity ratios (VR) were 10 and 20. All test conditions other than the velocity ratio were the same for the two cases. The notable difference between these two flows can easily be seen. For the VR=20 case, the mean flow was symmetrically distributed across the duct, while for the VR=10 case, the mean flow always followed either the top or the bottom wall and hence was significantly asymmetrical. It should be noted that there was no noticeable preference for the flow to follow either the top or bottom wall. A very small perturbation in the jet flow rates would cause the flow to switch from one wall to the other and it occasionally switched spontaneously. The data shows that there was very little decay in the wall-following jet velocity in the downstream direction in the VR=10 case. Furthermore, unlike the VR=20 case, zones of very high turbulence were not found in the flow field for the VR=10 case. Instead, a well-defined shear layer extending far downstream of the jet injection station was indicated. Therefore, it seems safe to conclude that the primary and secondary flows were poorly mixed in the VR=10 case. Another undesirable characteristic of a wall-following flow is the uneven heating load on the combustor walls. For these reasons, a velocity ratio of 20 would be preferable to a velocity ratio of 10 for combustor operation.

Figure 11 shows a comparison of two test cases where the jet injection angle was varied from 90° to 120°. All test conditions other than the jet injection angle were the same for the two cases. The behavior of these two flows downstream of the jet injection point was very similar, but the distribution of turbulence around the jets indicated that 120° injection causes higher turbulence near the duct walls while 90° injection causes higher turbulence near the center of the duct. While it would be difficult to conclude that one injection scheme is definitely better than the other, 90° injection would probably be preferred since higher turbulence level regions should correspond to regions of more intense mixing and combustion and it is desirable to

keep the hottest part of the flow in the center of the duct.

Figure 12 shows a comparison of three test cases with duct area reductions of 0% (no reduction), 25% and 50%. All test conditions other than the size of the area reduction were the same for the three cases. The decay of jet velocity near the injection point was similar for all three cases. Substantial recirculation existed downstream of the injection plane in the 0% restriction flow but was somewhat shorter downstream of the injection plane in the 25% restriction flow. Remarkably, there was no indicated recirculation downstream of the jet injection plane in the 50% area restriction case. Turbulence data indicates that the flow was very uniformly mixed by the time it left the restriction in the 50% case, but was still mixing in the 0% and 25% cases. A reasonable conclusion is that a restriction downstream of the jet injection point shortens the extent of the downstream recirculation zone. A 25% area reduction causes some shortening in the recirculation, but a 50% area reduction is more effective and would probably allow for a shorter secondary combustor with less gas-to-combustor-wall heat loss.

SUMMARY

A 1/6 scale water flow model of the Low Mass Flow secondary combustor was tested in order to determine the effects of combustor geometry and combustion air injection techniques on the flow and mixing in the secondary combustor. A dual Bragg cell laser velocimeter was used to obtain detailed two-component velocity data for five model configurations. In the study air flow injection angles of 90° and 120° (relative to the bulk flow direction), velocity ratios of 20/1 and 10/1, and cross-sectional area reductions of 50%, 25% and 0% were tested. The following conclusions were drawn from the results of this study:

1) A bulk velocity ratio of 20 between the secondary jets and the primary stream provides a shorter, more intense mixing region with more uniform mixing across the duct than a velocity ratio of 10 for secondary combustor operation.

2) For the cross flow injection type combustor considered, test results did not indicate clear-cut advantages for either 120° or 90° injection. Injection at 120° results in greater turbulence near the combustor walls while 90° injection provides greater turbulence near the combustor centerline; hence, 90° injection could provide a less severe environment for the walls of the combustor. However, the test results do not support a firm conclusion in this regard.

3) An area reduction downstream of the secondary air injection shortens the downstream recirculation. A 25% area reduction causes some shortening but a 50% area reduction eliminates recirculation downstream of the restriction, possibly allowing for a shorter combustor.

4) In all cases studied the flow had a periodic wake regime concentrated at the plane of symmetry, resulting from the alternate growth and shedding of vortices produced by the interaction of the injected and bulk flows. Strong oscillations with frequencies from 0.7 to 1.6 Hz were identified, but what determined the shedding frequency was not established (although some dependence on the duct area reduction was indicated.)

It has been shown, elsewhere, that data from subscale water flow models, scaled as in this study to match the bulk secondary to primary velocity and mass-flow-rate ratios, agree well with real combustor performance data. Therefore, conclusions from the cold flow model study are being used to define operational criteria for the CFFF secondary combustor, with due consideration given to the effects of density gradients produced by chemical reactions and the evolution and transfer of heat. For example,

the CFFF secondary combustor will be operated with injector velocity ratios near 20 rather than 10, and modifications to increase the injector plane area restriction will be considered.

REFERENCES

1) D. B. Spalding, "The Art of Partial Modeling", 9th Symposium (International) on Combustion, pp. 833 - 842, 1962.

2) A. E. Clarke, et al., "Some Experiences in Gas Turbine Combustion Chamber Practice Using Water Flow Visualization Techniques", 9th Symposium (International) on Combustion, pp. 878 - 891, 1962.

3) W. M. Farmer, et al., "Characterizing MHD Coal Combustor Particle Fluxes with Laser Velocimeters and Particle Sizing Interferometers", Proceedings of the 1981 Symposium on Instrumentation and Control for Fossil Energy Processes, ANL-81-62, CONF - 810607, Argonne National Laboratory, pp. 230 - 237, 1981.

4) J. P. Foote, "A Cold Flow Model Study of Turbulent Mixing in a Secondary Combustor", M.S. Thesis, The University of Tennessee, 1982. (Also United States Department of Energy Report DOE-ET-10815-87).

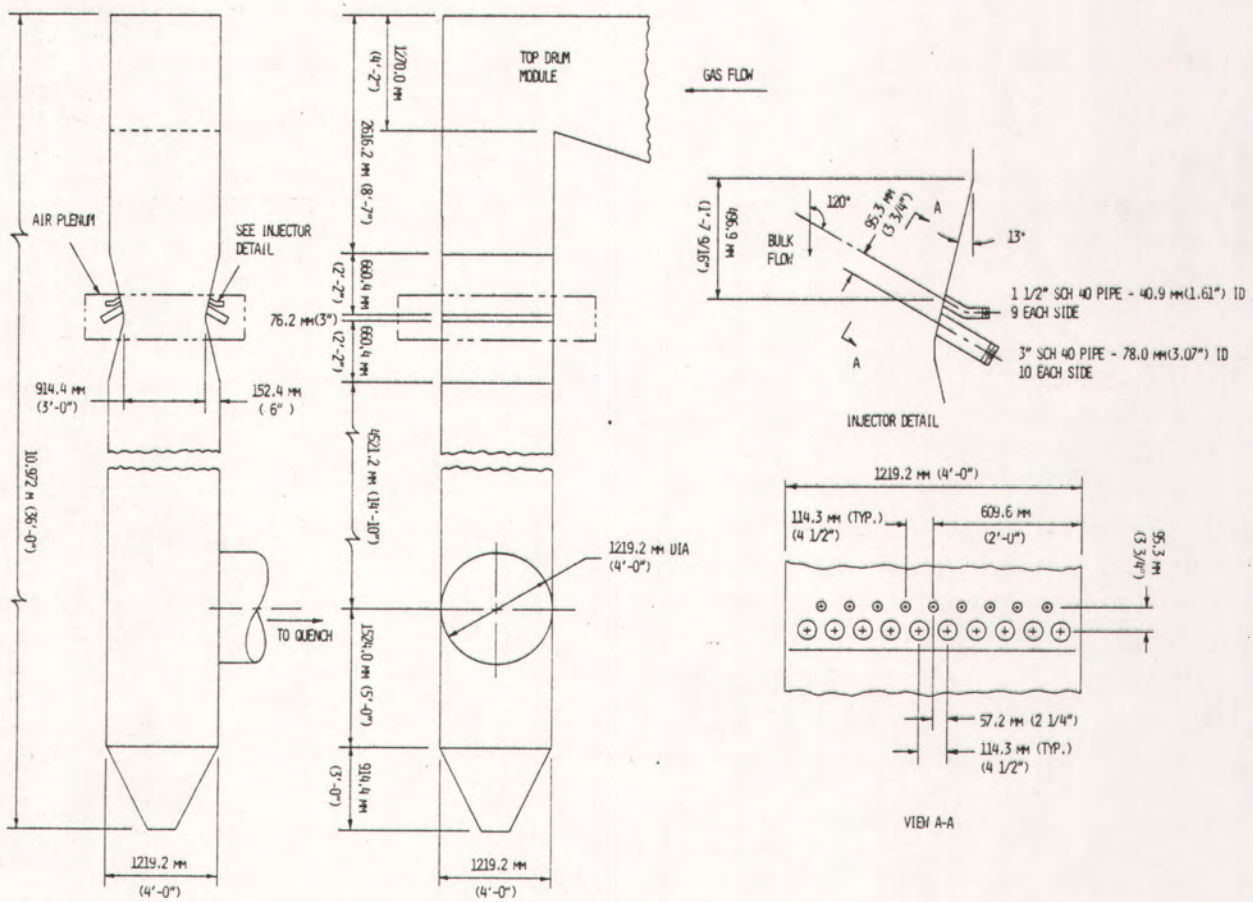

Figure 1. Secondary Combustor Schematic.

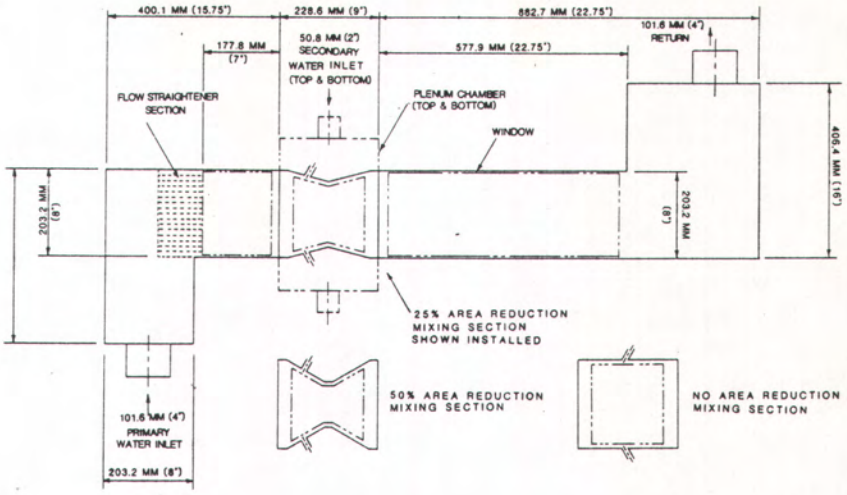

Figure 2. Water Flow Model Schematic.

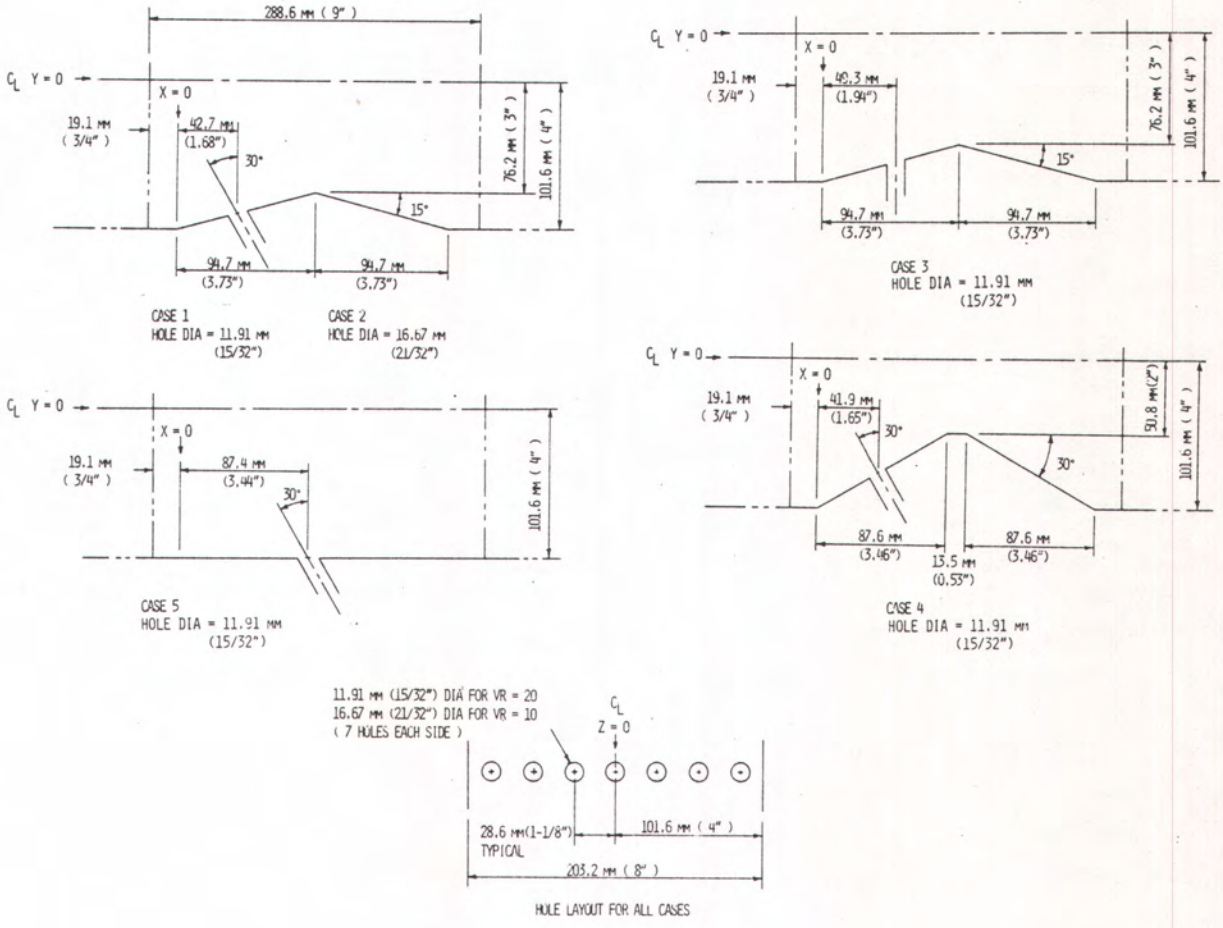

Figure 3. Model Test Configurations.

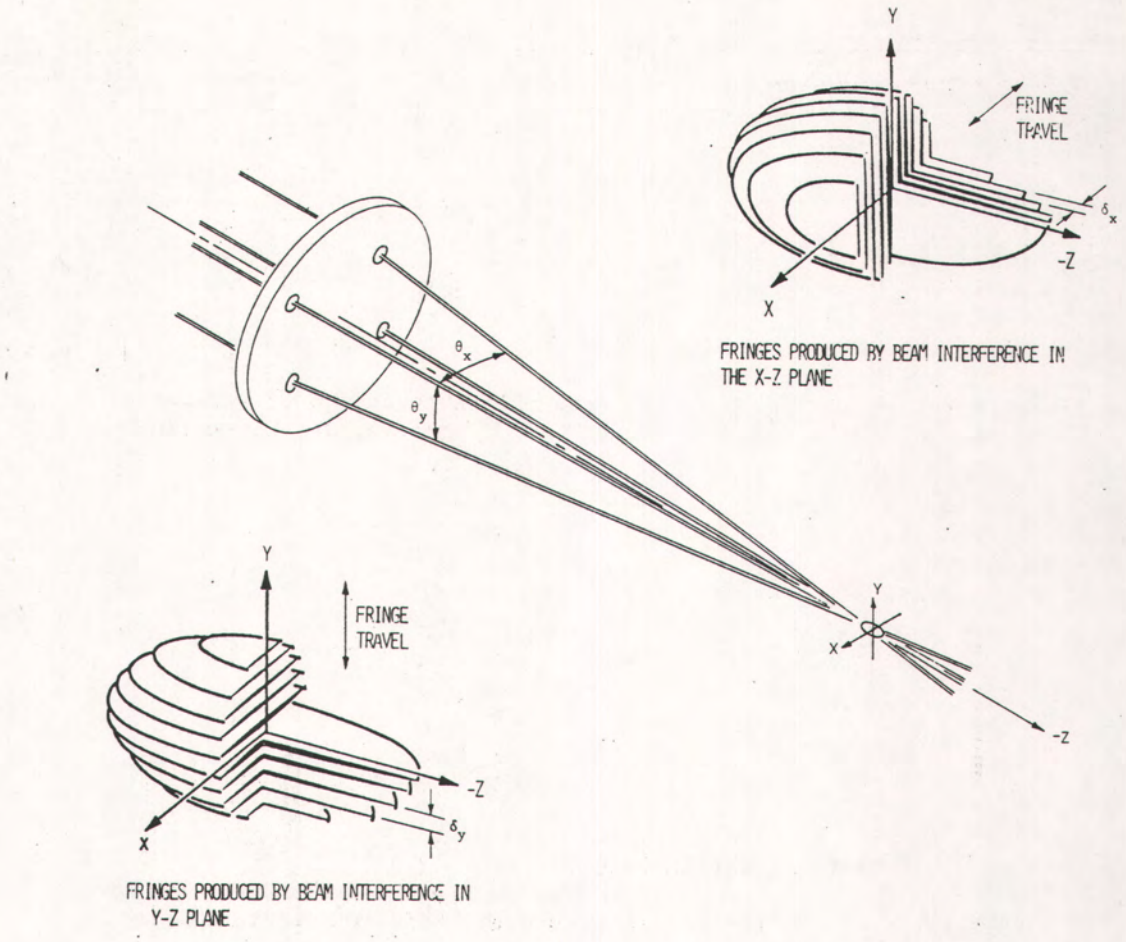

Figure 4. Laser Velocimeter Probe Volume.

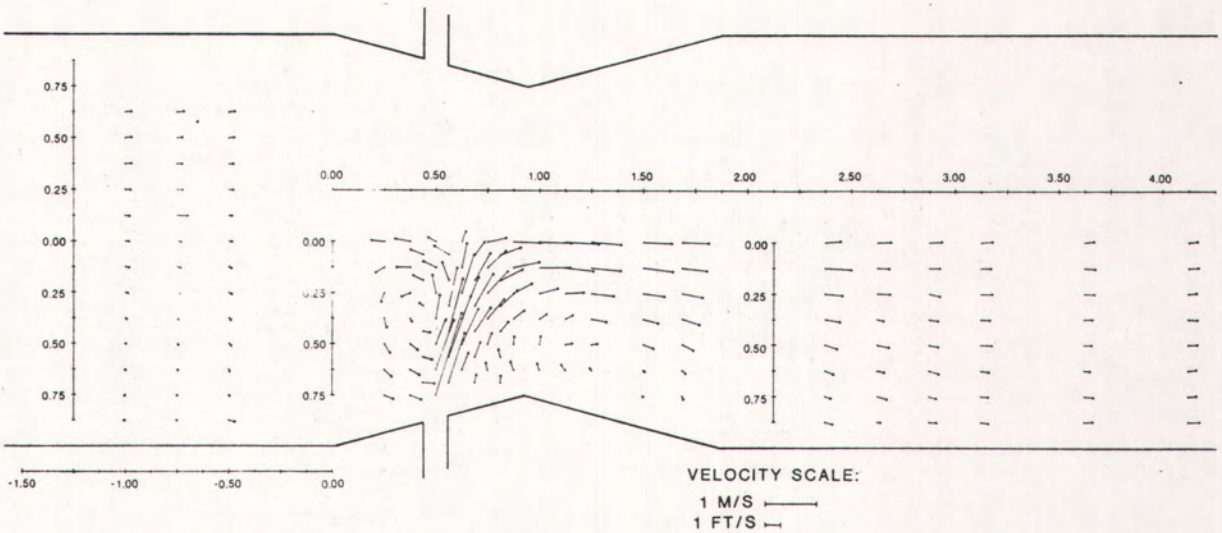

Figure 5. Velocity Field in Plane Bisecting a Jet. Jet Injection Angle = 90^0, Area Reduction = 25%, Mass Ratio = 0.75, Velocity Ratio = 20.

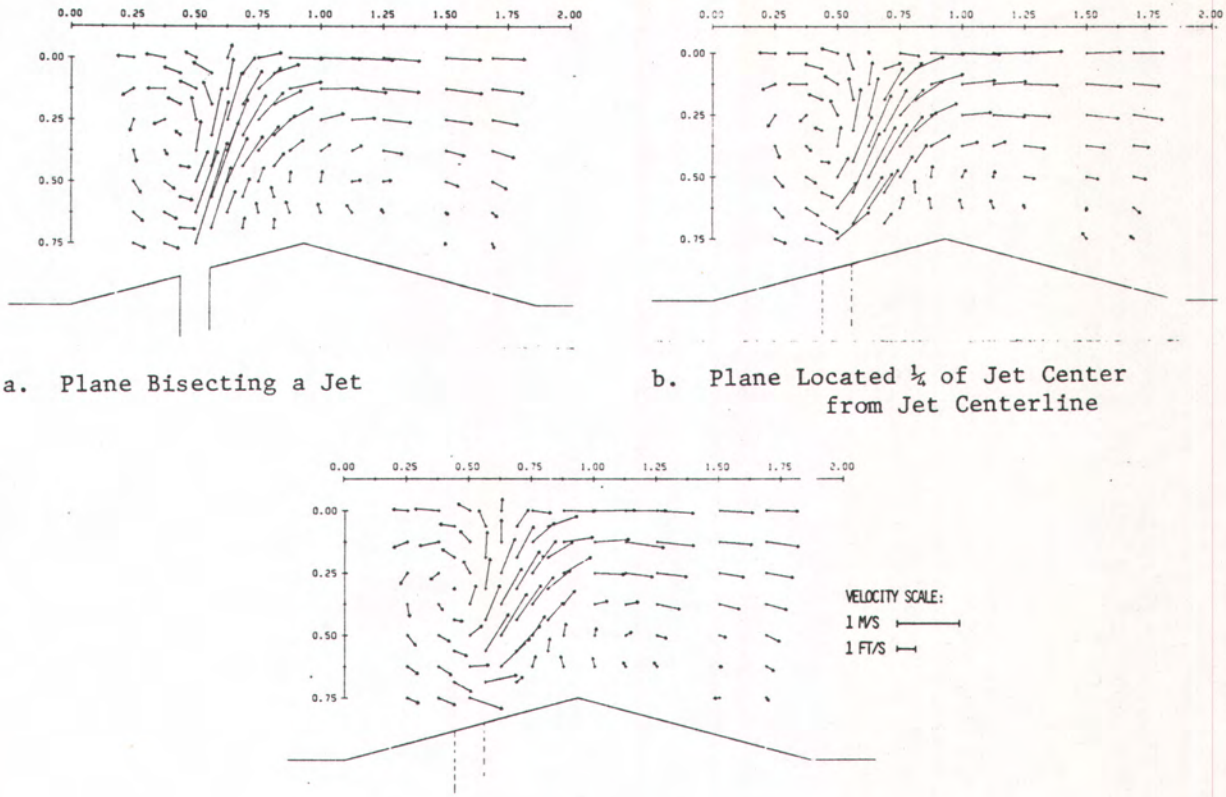

a. Plane Bisecting a Jet

b. Plane Located ¼ of Jet Center from Jet Centerline

c. Plane Midway Between Two Jets

Figure 6. Velocity Fields at Different Planes in the Jet Injection Region.

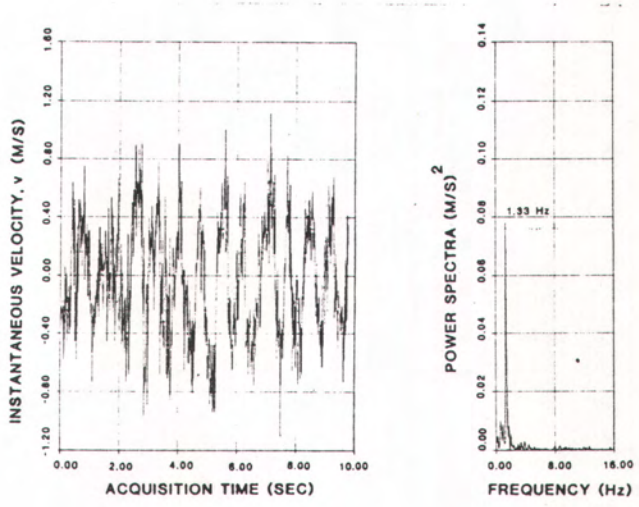

Figure 7. Vertical Velocity Component Variations in Time at X=1, Y=0, Z=0.

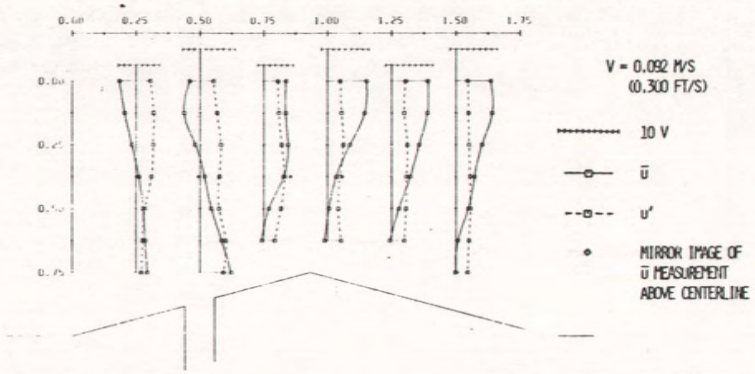

a. Axial Velocity and Turbulence Intensity Profiles

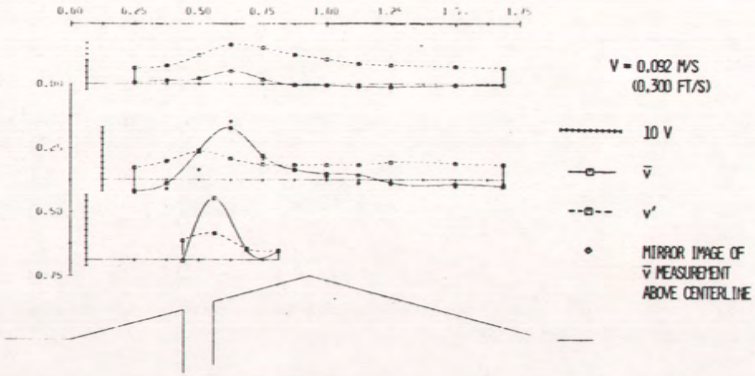

b. Vertical Velocity and Turbulence Intensity Profiles

Figure 8. Mean Velocity and Turbulence Intensity Profiles.

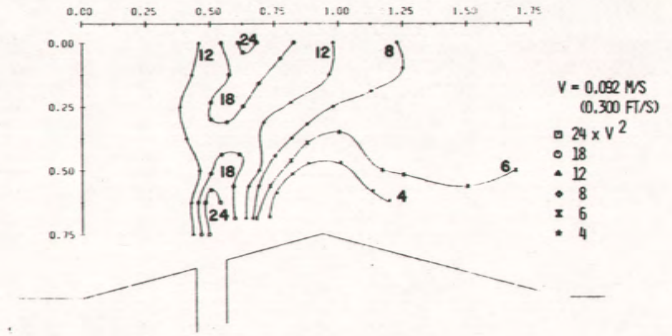

a. Turbulent Kinetic Energy, $(u'^2 + v'^2)/2$

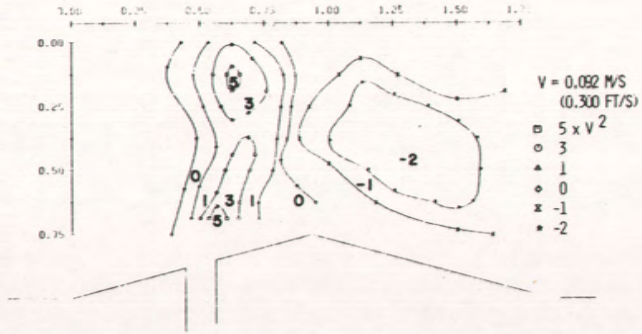

b. Reynolds Stress, $\overline{u'v'}$

Figure 9. Constant Value Contours of Turbulent Kinetic Energy and Reynolds Stress.

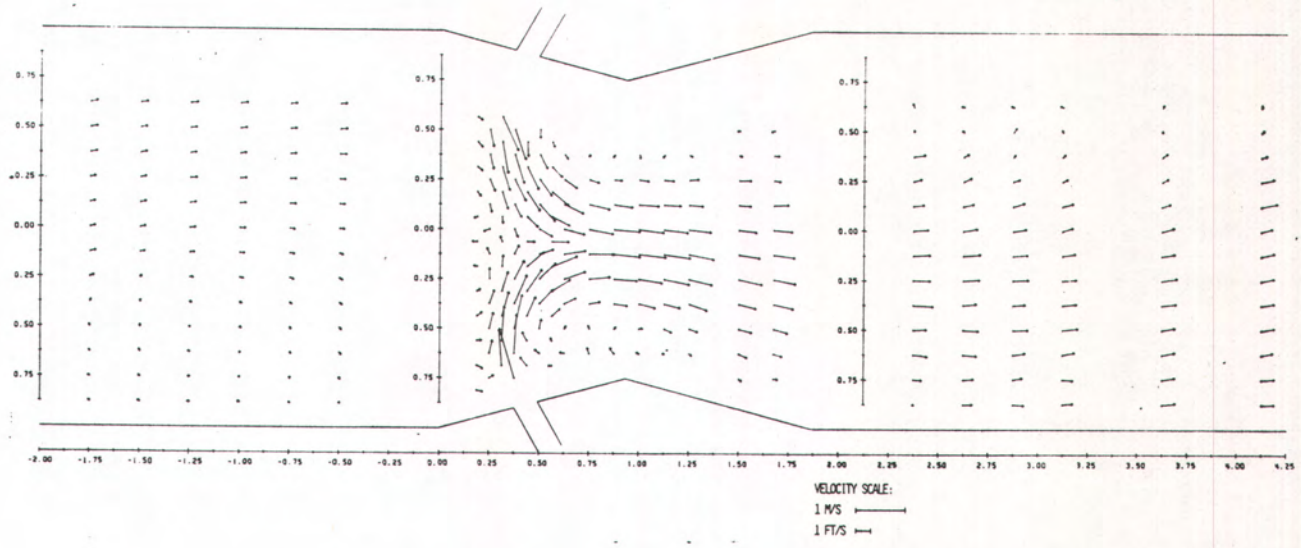

a) Injection Angle = 120^0, Velocity Ratio = 10, Area Reduction = 25%

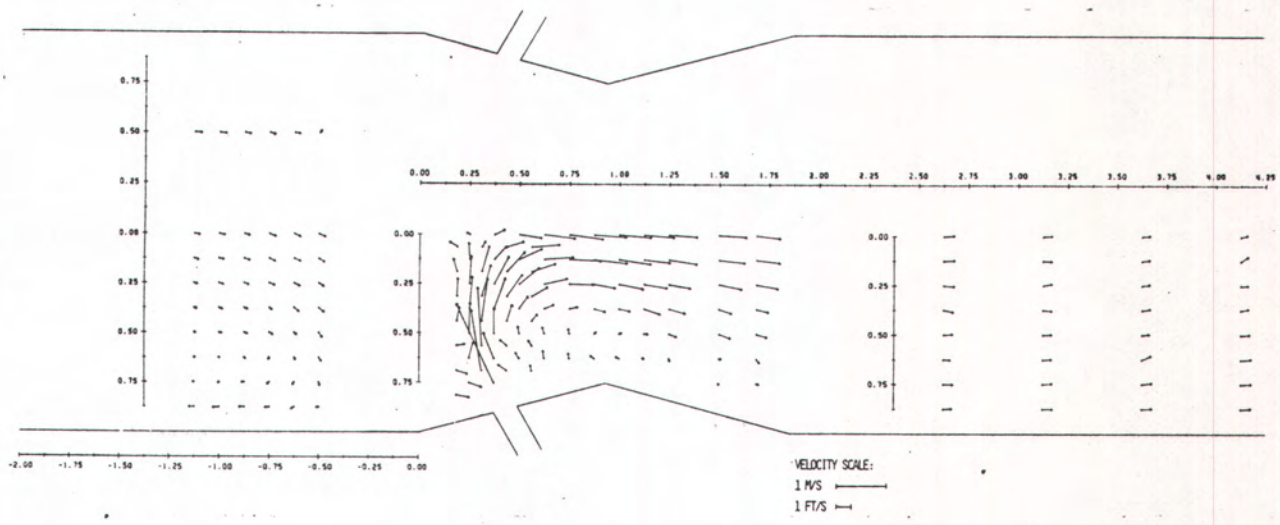

b) Injection Angle = 120^0, Velocity Ratio = 20, Area Reduction = 25%

Figure 10. Measured Flowfield Changes with Different Velocity Ratios.

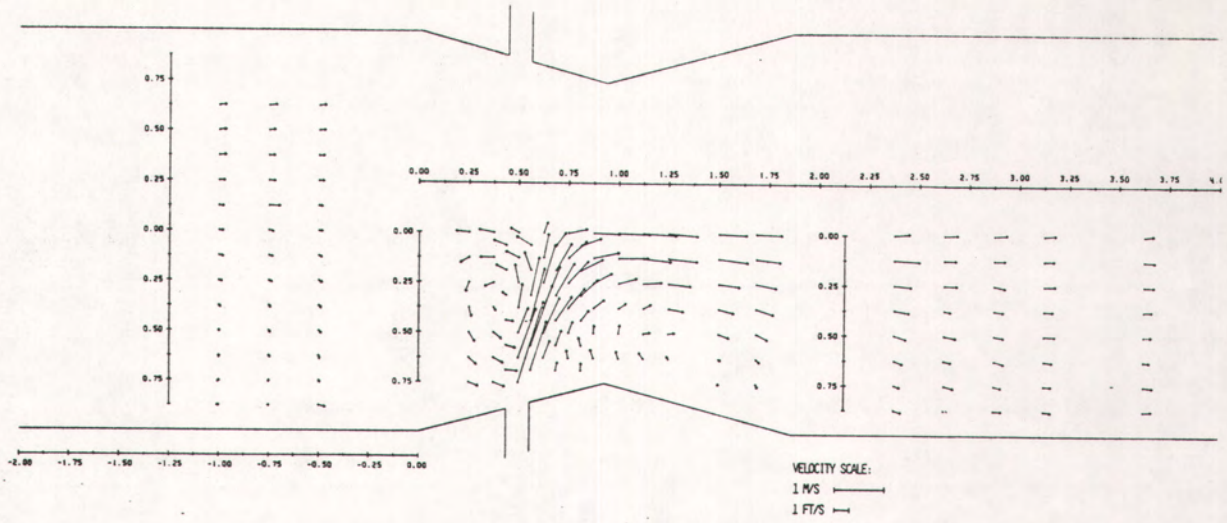

a) Injection Angle = 90^0, Velocity Ratio = 20, Area Reduction = 25%

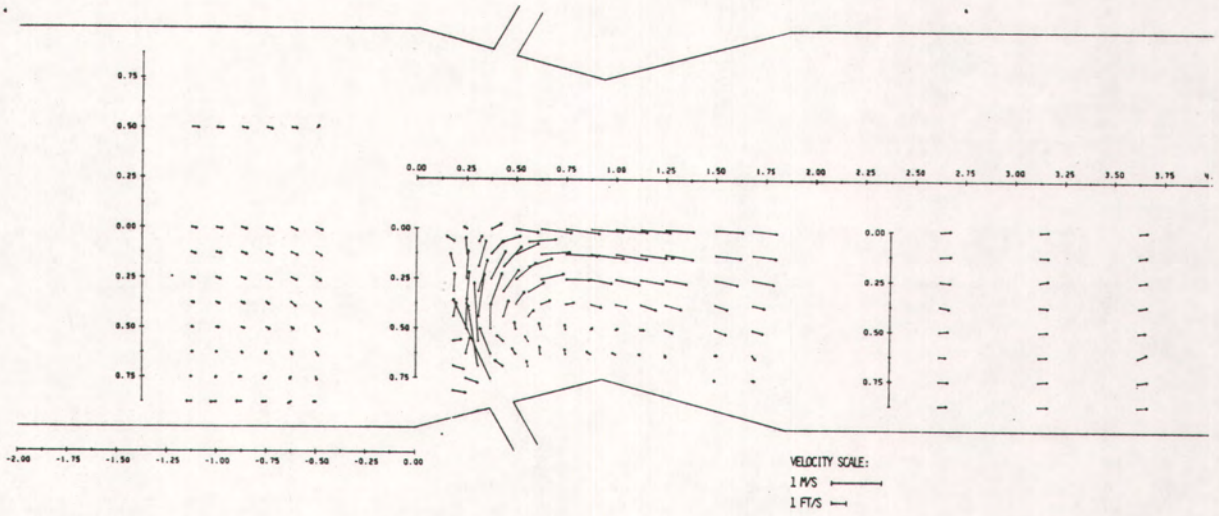

b) Injection Angle = 120^0, Velocity Ratio = 20, Area Reduction = 25%

Figure 11. Measured Flowfield Changes with Different Jet Injection Angles.

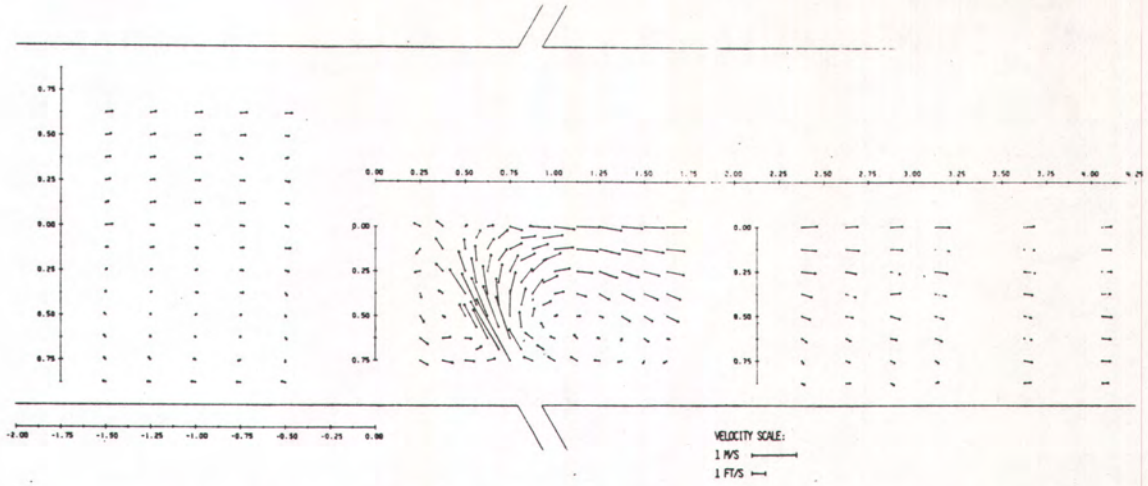

a) Injection Angle = 120^0, Velocity Ratio = 20, Area Reduction = 0%

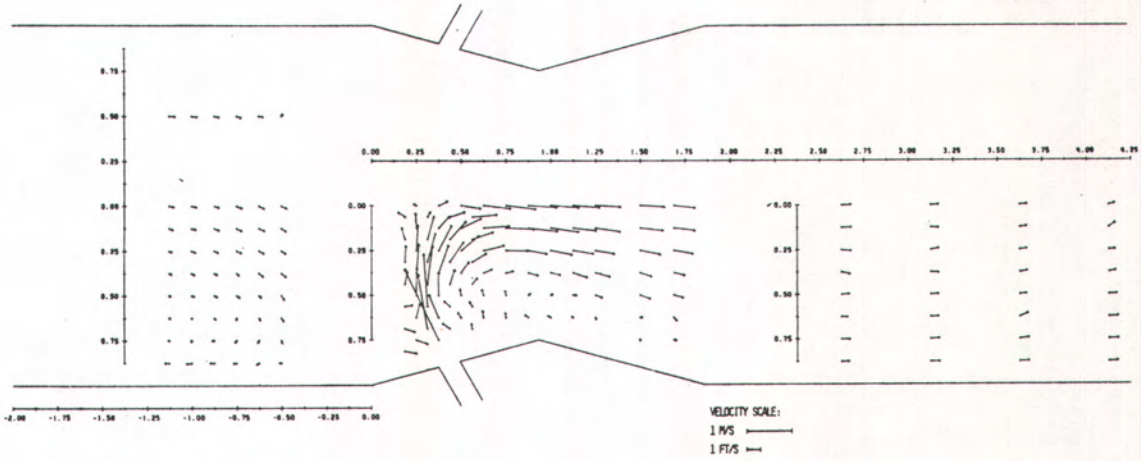

b) Injection Angle = 120^0, Velocity Ratio = 20, Area Reduction = 25%

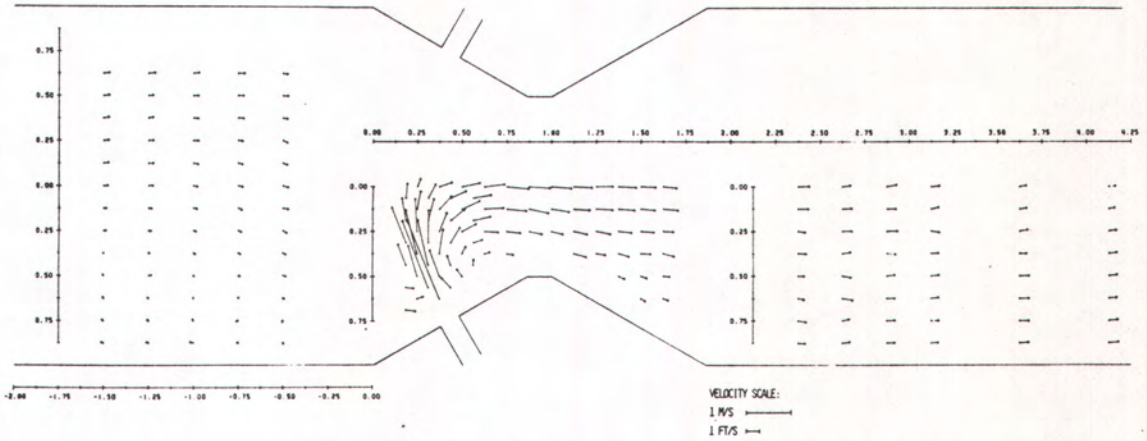

c) Injection Angle = 120^0, Velocity Ratio = 20, Area Reduction = 50%

Figure 12. Measured Flowfield Changes with Different Area Restrictions.